metals

MDPI

Article

Strategy Development for the Manufacturing of Multilayered Structures of Variable Thickness of Ni-Based Alloy 718 by Powder-Fed Directed Energy Deposition

Pedro Ramiro [1,*], Mikel Ortiz [1], Amaia Alberdi [1] and Aitzol Lamikiz [2]

[1] TECNALIA, Basque Research and Technology Alliance (BRTA), Paseo Mikeletegi 7, 20009 Donostia-San Sebastián, Spain; mikel.ortiz@tecnalia.com (M.O.); amaia.alberdi@tecnalia.com (A.A.)
[2] Department of Mechanical Engineering, Faculty of Engineering of Bilbao, University of Basque Country, Alameda de Urquijo s/n, 48013 Bilbao, Spain; aitzol.lamikiz@ehu.eus
* Correspondence: pedro.ramiro@tecnalia.com; Tel.: +34-946-430-850

Received: 12 August 2020; Accepted: 19 September 2020; Published: 24 September 2020

Abstract: In this study, a manufacturing strategy, and guidelines for inclined and multilayered structures of variable thickness are presented, which are based on the results of an own-developed geometrical model that obtains both the coating thickness and dilution. This model is developed for the powder-fed directed energy deposition process (DED) and it only uses the DED single-track cladding characteristics (height, width, area, and dilution depth), the overlap percentage, and the laser head tilting-angle as inputs. As outputs, it calculates both the cladding geometry and the dilution area of the coating. This model for the Ni-based alloy 718 was improved, based on previous studies of the single clad working both vertically and at an inclined angle, adding the equations of the single clad characteristics with respect to the main process parameters. The strategy proposed in this paper for multilayered cladding consisted of both adding an extra clad at the edges of the layer and using a variable value of the overlap percentage between clads for geometric adaptations. With this strategy, the material deposition is more accurate than otherwise, and it shows stable growth. Manufacturing a multilayered wall of wider thicknesses at higher heights was utilized to validate the strategy.

Keywords: directed energy deposition; powder; coatings; multilayer structure; variable thickness; geometrical model; deposition strategy; alloy 718

1. Introduction

Additive manufacturing (AM) is a technology that allows for the manufacturing of three-dimensional complex structures by adding material layer-by-layer. Under the term AM, different manufacturing methods can be distinguished, such as: directed energy deposition (DED), selective laser melting (SLM), binder Jetting, metal jetting, sheet lamination, photo-polymerization, and extrusion, as reported by Mehrpouya et al. [1]. Each of these processes is used to deposit different types of materials that are based on the energy source. Polymers, engineering plastics, ceramics, metals, metallic oxides, and metallic alloys are the most common materials used in AM processes. AM is attracting increasingly interest in various industries, such as biomedical [2], aerospace, or automotive.

Powder-fed directed energy deposition (DED) technology, also known as laser metal deposition (LMD) or laser cladding [3], is an AM process that directs a laser beam at a metallic substrate to produce a melt pool where material is injected in powder form. The powder mass flow is fused, and a high-quality metallurgical bond solidifies between the substrate and the added material. Therefore, the part can be built up layer by layer for the manufacture of complex geometrical forms.

This technology produces near-net-shape geometries that must be finished with a machining process. Nowadays, the hybridization of both AM and the machining process means that these processes may be combined in a single multitask machine, which increases the productivity and flexibility of the process.

The geometric uncertainty of the additive process in the machining operations with the tool is one of the most relevant challenges of hybrid manufacturing, as Cortina et al. [4] commented. Although there have been significant advances with numerical simulations, a complete model considering all stages and process parameters is still a complex procedure and far from the real status, as explained by Tamanna et al. [5]. In addition, the computational cost of a simulation is unclear. The simplest geometrical simulation can take hours, as reported by Salonitis et al. [6], whose laser cladding simulation for prediction of residual stresses and part distortion took 6 h of CPU time on a 12-processor desktop computer.

The numerical models that are presented in the literature can predict mechanical properties, structure, and defects. Arrizubieta et al. [7] predicted the geometry, grain size, hardness, and porosity of a ring of DED-manufactured AISI 304 stainless steel. Wei et al. [8] simulated the three-dimensional grain growth during multi-layer printing of Inconel 718. The work of Lu et al. [9] predicted residual stresses and distortion on rectangular and S-shaped parts of Ti-6Al-4V. However, the processing parameters must be defined before the modeling and simulation process. Most users, such as Dass et al. [10], relied on expensive and time-consuming techniques for process parameter optimization, such as multiple experimental runs. In experimental based optimization techniques, it is common practice, due to the large number of processing parameters, to keep some of those parameters unchanged, in an attempt to speed up the optimization process. However, applying that approach to Ti-6Al-4V parts led Azarniya et al. [11] to conclude that it entailed systematic uncertainties, which the numerical models could not clarify, due to the complexity of the process.

The vertically deposited single clad is normally considered to be a fundamental pillar for obtaining the map of process parameters, as shown in the work of de Oliveira et al. [12]. The objective is to select one or more conditions for further studies of the overlap clad, as done in previous works using Eutroloy 16606A as a filler material [13] and by laser cladding of multilayer walls reported by El Cheikh et al. [14] and Arregui et al. [15]. However, there is no viable experimental argument for rejecting single clad parameters that are based on overlap percentages or multilayer structures. In addition, the same parameters for vertical and inclined deposition are assumed in most works, e.g., in the study of Möller et al. [16], despite it being demonstrated by Hao et al. [17] that the clad characteristics changed with the tilting angle.

Most of the literature on geometrical laser cladding models is focused on single clad geometry, such as in the work of Bax et al. [18] and El Cheikh et al. [19] and the overlap percentage, such as in the works of Chen et al. [20] and Zhang et al. [21]. Nevertheless, there is no model for multilayer structures of variable thickness. These types of structures are required when manufacturing or repairing complex geometries.

The deposition strategy is an area of study in the DED process that strongly depends on the kinematic configuration of the DED machine and the type of nozzle [4]. Although there are nowadays specific modules in several Computer Aided Manufacturing (CAM) software packages for the AM process, their effectiveness is unclear. It is necessary to develop a specific CAM program depending on the complexity of the deposition geometry, which adapts the trajectory to the "rules and monitoring system" of each additive manufacturing system, as done by Garmendia et al. [22]. Additionally, the strategy of deposition is critical for obtaining a good geometry, as demonstrated by Kono et al. [23].

The present work focused on the development of guidelines and a deposition strategy for the manufacturing of multilayered structures of variable thickness made of Alloy 718 by powder-fed DED. The strategy consists of both employing a variable overlap percentage and clad numbers per layer for adaptation to the profile of the structure and adding "extra material" on the edges, at certain layers,

to assure a stable growth. The development of this strategy is based on a geometrical model of coatings that was introduced in previous works [24,25], which allows, as a function of the employed process parameters, to define the optimal overlap percentage and clad numbers for each layer and predict the quantity of extra material that is needed for the edges of the geometry. The utility of this model was previously demonstrated for the manufacturing of straight walls. The strategy that is presented in this work is validated by means of manufacturing an inclined wall of variable thickness, featuring wider thicknesses at higher heights.

2. Materials and Methods

2.1. Background

The development of the deposition strategy for multilayered structures of variable thickness that is proposed in the present work is based on developments and knowledge acquired from the studies of previous works [24,25]. In this sense, three previously validated steps are described in the following subsections in order to introduce the knowledge that forms the basis of the present work:

1. The development of a geometrical model for overlapped clads (see Section 2.1.1.).
2. The development of an optimized deposition strategy for straight walls based on the geometrical model results (see Section 2.1.2.).
3. The influence of the main process parameters and nozzle tilting angle on the deposition process and the geometrical model for overlapped cladding (see Section 2.1.3.).

2.1.1. Coatings: Overlapped Clad Geometrical Model

The mentioned geometrical model serves to predict both the overlapped clad geometry and dilution area of coatings. On the one hand, the overlapped clad geometry is based on the model that was developed by Ocelík et al. [26], supposing that a feature of each new clad of the coating assumes a second-degree parabolic shape. This model achieved a high level of accuracy by taking into account purely geometrical parameters, such as the characteristics of the single clad (Figure 1) and the overlap percentage (d_o) of the coating. On the other hand, the dilution area of the coating can be obtained from the experimental results of previous works [13,27,28]. The model employs the single clad characteristics (h, w, p, and A) as inputs (Figure 1b) and it assumes that the coating (Figure 2a) is the sum of the clads deposited at the overlap distance. The model was developed to predict the cross section of a coating fabricated with the zig-zag strategy perpendicular to the feed direction (Figure 2b).

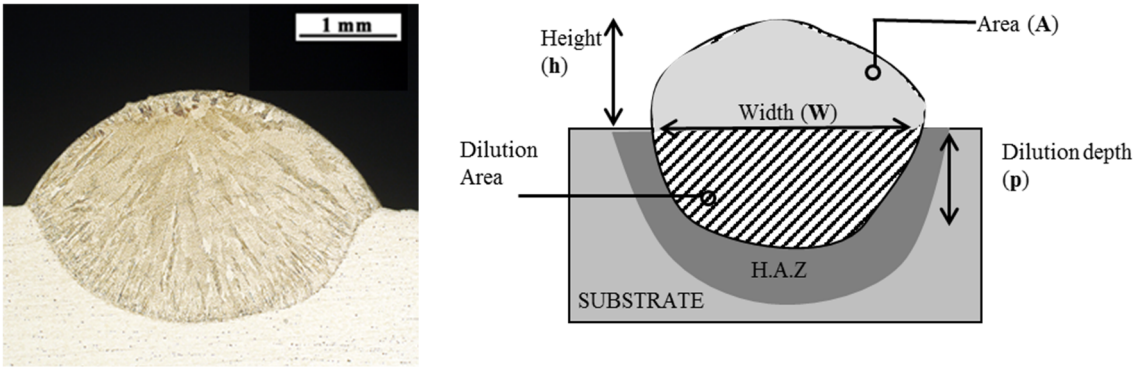

(**a**) (**b**)

Figure 1. Single clad. (**a**) Macrophotograph of a cross section of a single clad; (**b**) scheme of the single clad characteristics.

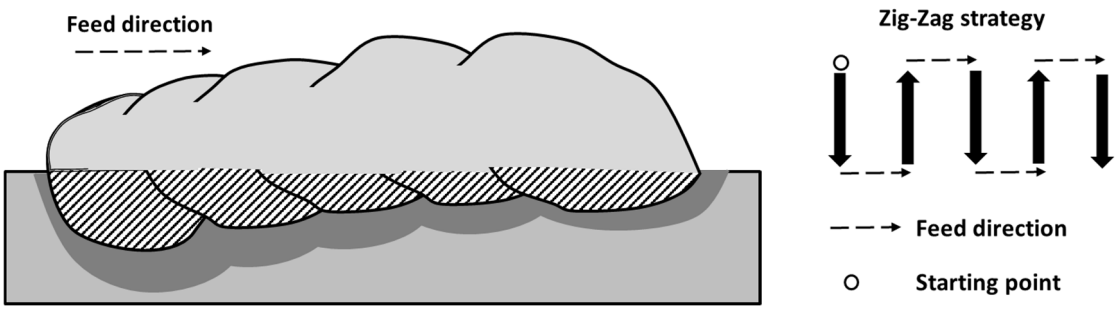

Figure 2. Overlapped clad deposited with the zig-zag strategy: (**a**) scheme of the final cross section of the coating; (**b**) scheme of the zig-zag strategy.

The model supposes that each new clad is deposited with the same area as the single clad (Figure 3a), forming a new clad $i + 1$ with the overlapped area of the previous clad i (Figure 3b). Clad $i + 1$ has a second-degree parabola shape with a width (w_{i+1}). It is calculated by assuming that the height, Y_i, at the overlap point, P, is the same as for the previous clad (clad i), that the area from the origin O_{i+1} to P (A') is the sum of the single clad area (A) plus the overlapped area (A_o) of the previous clad i, that the distance from the origin O_{i+1} to P is the same as the single clad width (w), and that the distance from origin O_{i+1} to O_i is the overlap distance of the single clad width (D_o). The equations of the second-degree parabola are obtained from the origins O_{i+1} and O_i, rather than the central axis, because the equations are more easily solved. In the first iteration, clad i is the single clad.

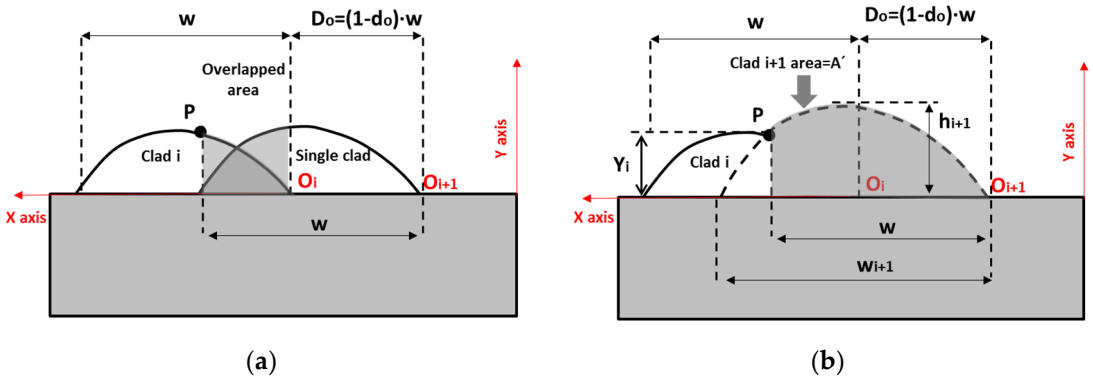

Figure 3. Geometrical model. (**a**) First iteration clad; (**b**) adjacent clad $i + 1$: second-degree parabola formed with the single clad area and the overlapped area of the previous clad i.

Equations (1) and (2) are solved to define the features of clad i with respect to origin O_i and, likewise, Equations (3) and (4), to establish the geometry of the adjacent clad ($i + 1$) with respect to origin O_{i+1}. Equations (5)–(13) are solved to find clad $i + 1$ and begin a new iteration.

$$Y_i = a_i \times x^2 + b_i \times x \tag{1}$$

$$A_i = \frac{a_i \times x^3}{3} + \frac{b_i \times x^2}{2} \tag{2}$$

$$Y_{i+1} = a_{i+1} \times x^2 + b_{i+1} \times x \tag{3}$$

$$A_{i+1} = \frac{a_{i+1} \times x^3}{3} + \frac{b_{i+1} \times x^2}{2} \tag{4}$$

$$a_i = -\left(\frac{4 \times h_i}{{w_i}^2}\right) \tag{5}$$

$$b_i = \frac{4 \times h_i}{w_i} \tag{6}$$

$$Y_i = a_i \times (d_o \times w)^2 + b_i \times (d_o \times w) = a_{i+1} \times w^2 + b_{i+1} \times w \tag{7}$$

$$A' = A_o + A = \frac{a_{i+1} \times w^3}{3} + \frac{b_{i+1} \times w^2}{2} \tag{8}$$

$$A_o = \frac{a_i \times (d_o \times w)^3}{3} + \frac{b_i \times (d_o \times w)^2}{2} \tag{9}$$

$$a_{i+1} = 3 \times \left(\frac{A}{w^3} - \frac{b_{i+1}}{2 \times w} \right) = -\left(\frac{4 \times h_{i+1}}{{w_{i+1}}^2} \right) \tag{10}$$

$$b_{i+1} = 2 \times \left(\frac{3 \times A}{w^2} - \frac{Y_i}{w} \right) = \left(\frac{4 \times h_{i+1}}{w_{i+1}} \right) \tag{11}$$

$$h_{i+1} = -\left(\frac{{b_{i+1}}^2}{4 \times a_{i+1}} \right) \tag{12}$$

$$w_{i+1} = -\left(\frac{b_{i+1}}{a_{i+1}} \right) \tag{13}$$

The solving of the height and width equations of clad $i + 1$ (Equations (12) and (13)) is the starting point for another iteration. The effective thickness of the coating, which is the thickness to obtain a constant coating after machining, is defined by the lower thickness calculated by the model. Thus, it corresponded to the lower value of Y_i that was obtained in the overlapped point P of all the clads that formed the coating. The height of each overlapped clad of the coating can be considered as the reference to guide the machining process.

Moreover, the model simplifies the real dilution of the clad (Figure 4a) to a second-degree parabola on the substrate (Figure 4b) of the same width as the single clad. Likewise, it is assumed that the sum of the height and dilution depth remains constant in all of the clads that form part of the coating (Equation (14)). Thus, any increase in the overlap percentage lowers the dilution, because a part of the energy that is required to melt the substrate is employed to melt the overlapped part of the previous clad. This assumption is a simplified constant value of the energy balance between the deposited material and the melted substrate that was studied by Chakraborty et al. [29]. It was obtained by analyzing all of the fabricated coatings in previous works with different nozzles, metallic powders, and substrates [13,27,28].

$$h_i + p_i = h_{i+1} + p_{i+1} \tag{14}$$

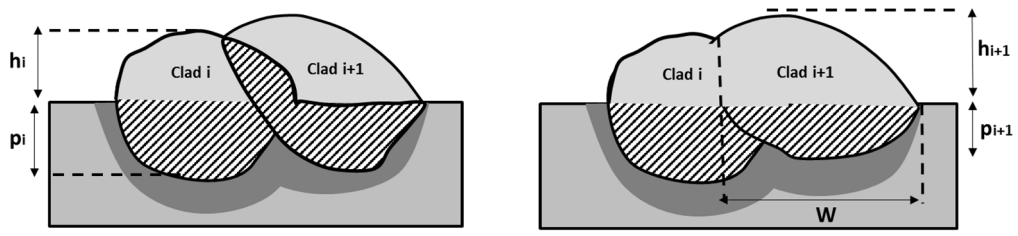

(**a**) (**b**)

Figure 4. Scheme of the dilution of the adjacent clad $i + 1$. (**a**) Real; (**b**) model.

The effectiveness of the model was validated with Eutroloy 16606A coated cross sections, analyzed in previous works [13,27], and deposited through a continuous coaxial nozzle with a slit of 1 and 0.5 mm (Figure 5a,b). In that case, it was possible to predict lack of fusion, due to a large amount of material in the overlapped zone governed by the overlap percentage, as shown in Figure 5b.

The cross-sections that were coated with Alloy 718 using a four-stream nozzle also validated the model (Figure 5c) [24].

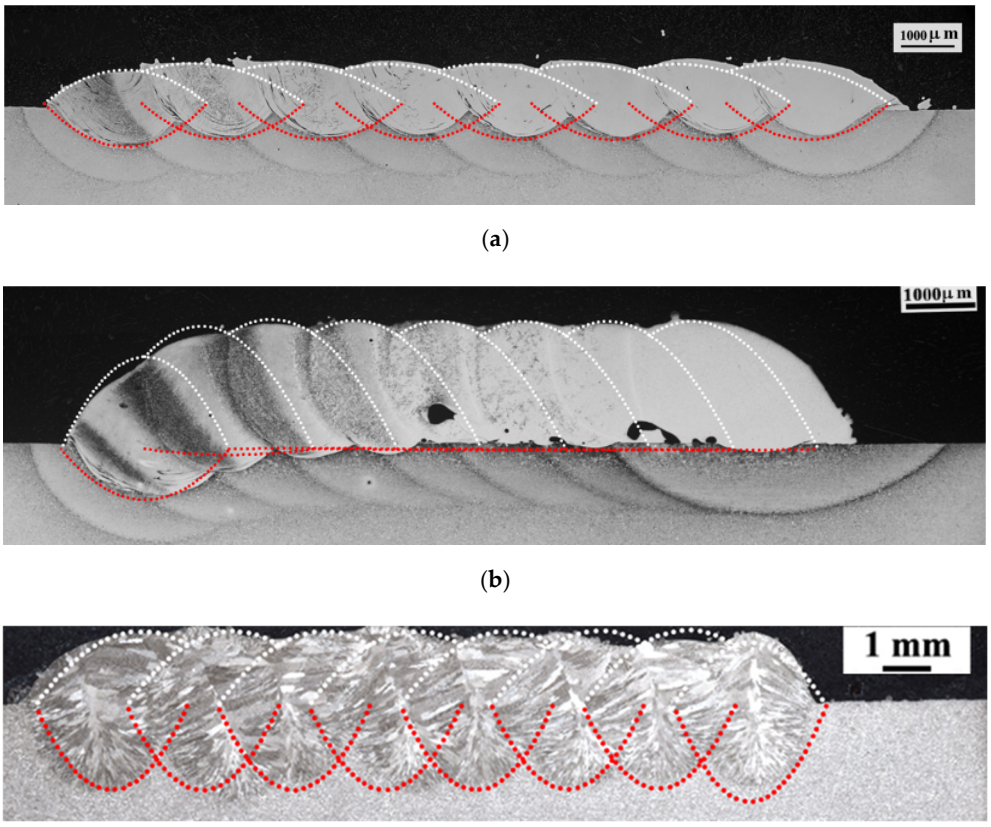

Figure 5. Comparison of the model with cross sections of real coatings: (**a**) coating of Eutroloy 16606A at 2700 W, 900 mm·min^{-1}, 15.6 g·min^{-1}, d_o = 40% and continuous coaxial nozzle with a slit of 1 mm; (**b**) coating of Eutroloy 16606A at 2100 W, 500 mm·min^{-1}, 12.3 g·min^{-1}, d_o = 50% and continuous coaxial nozzle with a 0.5 mm slit; and, (**c**) coating of Alloy 718 at 2500 W, 500 mm·min^{-1}, 18 g·min^{-1}, d_o = 40% and four-stream nozzle.

2.1.2. Deposition Strategy Optimization for Straight Walls

When fabricating a multilayer structure, a relevant aspect to consider is that the coating thickness of each layer increases from the first clad until it reaches a constant thickness. In addition, the last clad presents a sharp curve from the top to the substrate. Both of the situations generate a lack of material and a distortion at the edges (Figure 6a), which increases at higher numbers of layers, as shown by Nenadl et al. [30]. Thus, one possible solution to compensate for this absence of material is to add extra clads at the edges of the layer. In this sense, the model that is presented in the previous Section 2.1.1. can be used to predict this lack of material and the area needed at the edges of the layer to obtain constant vertical growth. Excluding the shape and waviness of the deposited material and only taking into account the deposited area within the overlapped parts of the model, the growth per layer (H_L) could be determined as the constant thickness obtained, assuming a coating formed by rectangular blocks of the same area (Figure 6b). This assumption allows for determining the extra clad area as the area that is needed to obtain a constant thickness at each edge and it can be expressed as a percentage of the single clad area (Figure 7). Employing the same parameters for all clads of the coating, this extra clad area percentage depends on the overlap percentage employed, increasing the area needed at higher overlap percentage values. This lack of material was not observed when fabricating the walls

with two overlapped clads per layer [25], because the amount of material that was deposited in the overlap area was distributed between both clads within the successive layers.

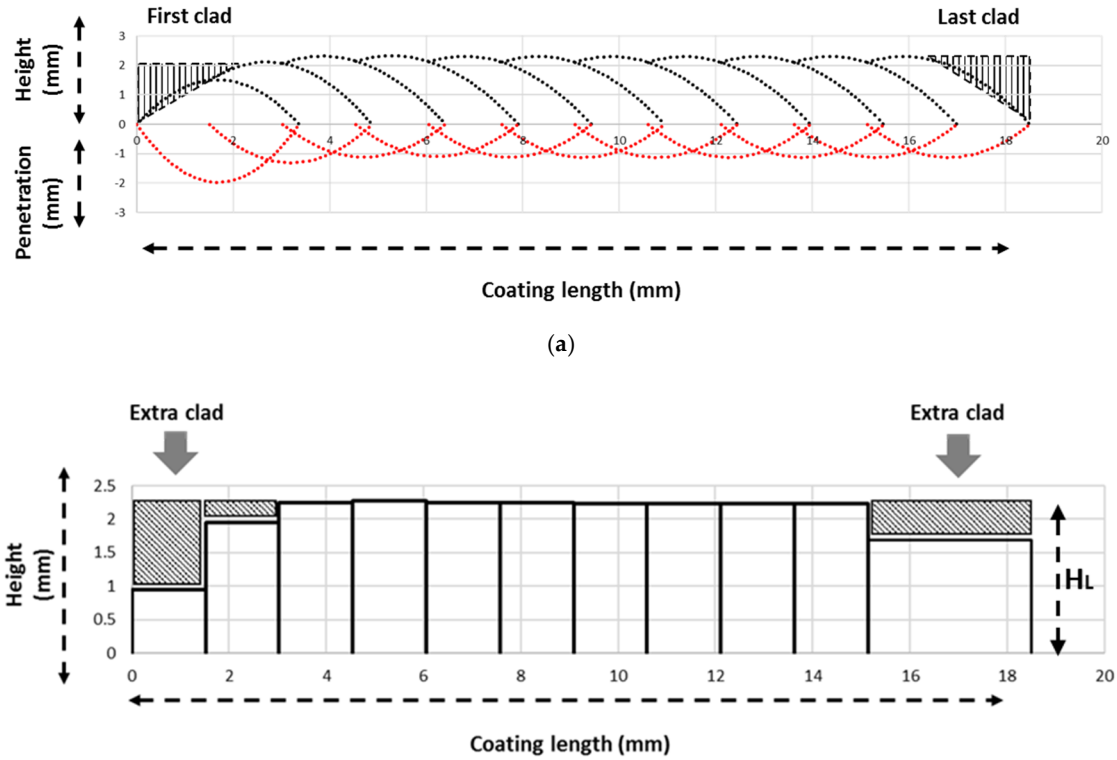

Figure 6. Lack of material predicted by the model at the layer edges. (**a**) Second degree parabola shape; (**b**) approximation to rectangular blocks.

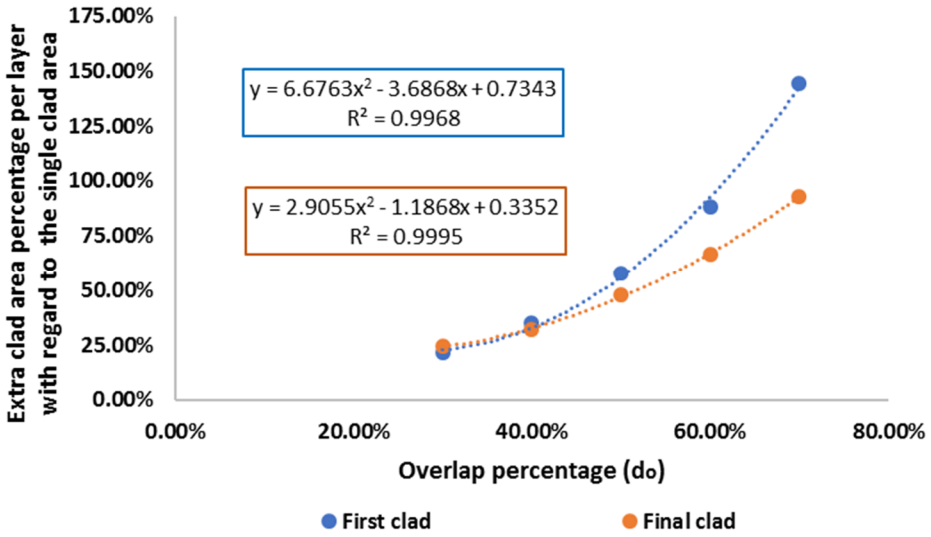

Figure 7. Representation of the extra clad area needed to compensate the lack of material on the edges of the coating as a function of the overlap percentage. Blue: area percentage needed in the first part of the coating; orange: area percentage needed in the final part of the coating. Data obtained from the coating model described in Section 2.1.1. for vertically deposited Alloy 718 at 2500 W, 18 g·min^{-1}, and 500 mm·min^{-1}.

The strategy for straight walls was validated in previous works [24], wherein two straight walls of Alloy 718, with a target cross-section of 12.9 × 15.6 mm^2, were deposited at an overlap percentage of 40% (Figure 8) with and without extra clads at the edges. An extra clad was added every two layers (maintaining the same laser power and powder mass flow rate) with twice the area per layer, in order to obtain an extra clad with a very similar feed rate to the clads that were coated. The wall deposited with the extra clad strategy presents a rectangular shape with no distortions at the edges, where more layers may be precisely deposited. On the contrary, the wall that is deposited without the extra clad presents a high distortion with a bullet shape. The distortion increases sharply at a higher number of layers. In addition to this loss of geometrical accuracy, there is an additional effect of increased distortion on the material deposition: a decrease in the powder efficiency. In fact, the powder efficiency of the structure with extra clads and without extra clads was, respectively, 60.1% to 52.4%.

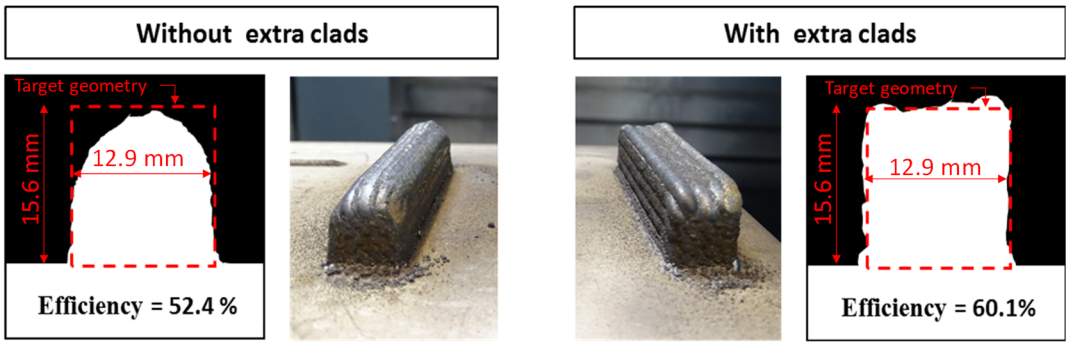

Figure 8. Straight wall results: (**a**) Cross-section without extra clad strategy; (**b**) Cross-section with extra clad strategy. The results from "Geometrical Model and Strategy in Single and Multilayer Structures Deposited by Powder-fed Directed Energy Deposition", by Ramiro et al. [24].

2.1.3. Influence of the Main Process Parameters and Tilting Angle

The geometrical model that is described in Section 2.1.1. uses the geometric characteristics of a single clad as input data, which are dependent upon the main process parameters (laser power, feed rate, and powder mass flow). In this sense, in previous work [25] Alloy 718 was characterized as a function of the main process parameters when vertically depositing (Equations (15)–(28)). Therefore, while applying this geometrical model, it is possible to obtain the resultant coatings of this material at a given laser power (P), feed rate (v), powder mass flow ($\dot{m}_p$), and overlap percentage within the range studied for the four-stream nozzle at a distance from the substrate of 14.5 mm [24] and with a laser spot size of 2.6 mm.

Height (h): Units W, mm·min^{-1} and g·min^{-1}; Equations (15)–(18).

$$h\ (mm) = \frac{A_h \times P}{v^2} + \frac{B_h \times \sqrt{P}}{v} + C_h \tag{15}$$

$$A_h = -2.4515 \times \dot{m}_p + 18.029 \tag{16}$$

$$B_h = 0.8638 \times \dot{m}_p - 0.322 \tag{17}$$

$$C_h = -0.0046 \times \dot{m}_p + 0.0431 \tag{18}$$

Width (w): Units W, mm·min^{-1} and g·min^{-1}; Equations (19)–(20).

$$w\ (mm) = \frac{A_w \times e^{(0.0022 \cdot P)}}{v} + 2.632 \tag{19}$$

$$A_w = -0.0135 \times \left(\dot{m}_p\right)^2 + 0.47 \times \dot{m}_p - 2.869 \quad (20)$$

Area (*A*): Units W, mm·min^{-1} and g·min^{-1}; Equations (21)–(23).

$$A\left(mm^2\right) = \frac{A_A \times (P - 526.34)}{v} - B_A \times (P - 1632) \quad (21)$$

$$A_A = -0.0031 \times \left(\dot{m}_p\right)^2 + 0.1431 \times \dot{m}_p - 0.8123 \quad (22)$$

$$B_A = -0.00001 \times \left(\dot{m}_p\right)^2 + 0.00037 \times \dot{m}_p - 0.0029 \quad (23)$$

Dilution Depth (*p*): Units KW, mm·s^{-1} and g·s^{-1}; Equations (24)–(28).

$$p\ (mm) = A_p \times C_p \times v + B_p \times D_p \quad (24)$$

$$A_p = -11.065 \times \left(\dot{m}_p\right)^2 + 6.302 \times \dot{m}_p + 0.1078 \quad (25)$$

$$B_p = -4.1886 \times \left(\dot{m}_p\right)^2 + 1.894 \times \dot{m}_p + 0.8176 \quad (26)$$

$$C_p = 0.0106 \times (P)^2 - 0.0609 \times P + 0.0323 \quad (27)$$

$$D_p = -0.2778 \times (P)^2 + 1.8937 \times P - 0.6502 \quad (28)$$

Apart from this, the characteristics of the single clad of Alloy 718 are also dependent upon the tilting angle (α) for material deposition, as previously demonstrated [25], reaching a maximum tilting angle of 30°. The results of tilting the nozzle when depositing on a horizontal substrate (Figure 9) should be considered for the manufacturing of walls of variable thickness, since, in this case this tilting is necessary and, as it was explained before, the single-clad characteristic change with the tilting. Thus, once the characteristics of vertically obtained clad (Equations (15)–(28)) are defined, the tilting angle may be used to calculate its effects on the clad characteristics.

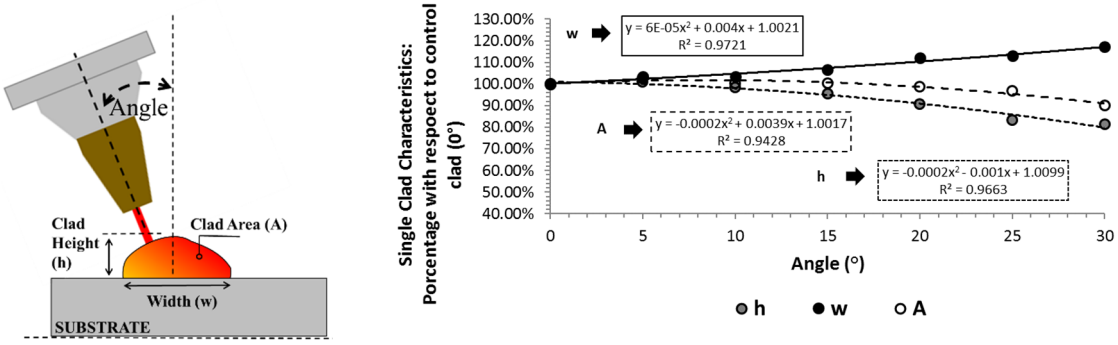

Figure 9. Effect of the head tilting on the single clad characteristics. Adapted from "Effects of Gravity and Non-Perpendicularity during Powder-Fed Directed Energy Deposition of Ni-Based Alloy 718 through Two Types of Coaxial Nozzle", by Ramiro et al. [25].

2.2. The Deposition of Multilayered Structures of Variable Thickness

The strategy for manufacturing a demanding geometry with a multilayer structure of variable and increasing thickness requires that several new aspects should be taken into account as compared to the straight wall case: the tilting of the nozzle, the single clad characteristics and their changing patterns with the tilting angle, and the maximum horizontal displacement that can be reached between layers (Δ*X*) [25]. Thus, the present work proposes a strategy that comprises the following steps for manufacturing multilayered structures of wider thicknesses at higher heights:

1. Selection of the optimum working conditions (P, v, $\dot{m}_p$) to manufacture the part.
2. Definition of the deposition trajectory featuring a variable overlap percentage and clad numbers per layer, while taking into account the maximum horizontal displacement (ΔX) admissible, for adaptation to the profile of the wall, thus preventing material deposition outside of the geometric design.
3. Adding "extra clads" on the edges of the layers to assure a homogeneous growth of the part.

In this sense, the geometrical model for overlapped clads (Section 2.1.1.) is directed in order to calculate both the optimal overlap percentage and clad numbers per layer and the area of "extra clads" needed on the edges. A variable thickness wall with one straight side and the other with a wall angle (θ) of 66° (Figure 10a) was designed, and fabricated on a horizontal substrate, for which a laser head tilting equal to the wall angle was used, in order to develop and experimentally validate the strategy (Figure 10b). Thus, a horizontal displacement per layer (ΔX) was programmed in order to obtain the correct angle with the growth per layer (ΔZ), as explained below in Section 2.2.2. The geometric model was calculated while taking into account the selected working conditions (P, v, $\dot{m}_p$) and the change of the single clad characteristics at the tilting angle ($\alpha = 90 - \theta$) with regard to the vertically deposited clad, using a tilted nozzle on a horizontal substrate, as explained in Section 2.1.3.

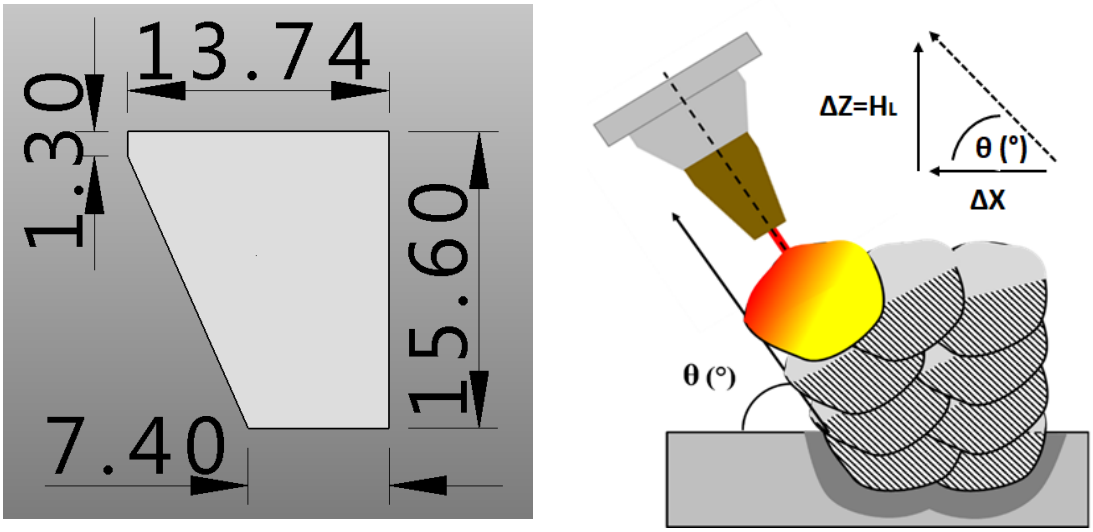

(**a**) (**b**)

Figure 10. (**a**) Cross-sectional dimensions of the target geometry employed for the development and validation of the deposition strategy for inclined walls of variable thickness; (**b**) scheme of the deposition strategy to validate. (unit: mm).

2.2.1. Experimental Set Up

A nickel-based alloy (Alloy 718) was used as both the filler and the substrate material in the experimental tests. The used filler material was in powder form with a granulometry between 45 and 150 µm, from Flame Spray Technologies (FST, Duiven, The Netherlands), and the substrate material was in an annealed state. Table 1 presents the chemical composition of the powder and the substrate materials. Alloy 718 presents excellent oxidation and corrosion-resistant properties at high-temperatures (up to 980 °C); hence, its widespread use in the aeronautical sector.

Table 1. Chemical composition of Alloy 718 powder and substrate (wt. %).

Material	Ni	Cr	Fe	Nb + Ta	Mo	Ti	Al
Powder	52.8	18.5	18	4.8	3.5	0.75	0.3
Substrate	53.5	18.7	17.7	5	2.9	0.94	0.58

All of the tests were performed on an IBARMIA ZVH45/1600 Add + Process hybrid machine (Figure 11a). This multiprocess machine (Ibarmia, Azkoitia, Spain) combines DED technology with a five-axis milling and turning (horizontal and vertical) capability. It is equipped with a Precitec YC52 cladding head (Precitec, Gaggenau, Germany), a Sulzer Metco TWIN-10-C Powder Feeder (Oerlikon Metco, Freienbach, Switzerland), and a Yb-Fiber Rofin FL030 3 kW Laser generator (Coherent Rofin, Santa Clara, CA, USA), with a continuous wavelength of 1.07 µm. The hybrid machine was fitted with a four-stream coaxial discrete nozzle from Precitec (Figure 11b). Working with the four-stream nozzle is the most efficient way to fabricate inclined walls on a horizontal substrate, as demonstrated in a previous work [25]. Tilting of the substrate was not contemplated, even though it would have avoided the gravity effects in the DED process, because it was not a feature of the machine.

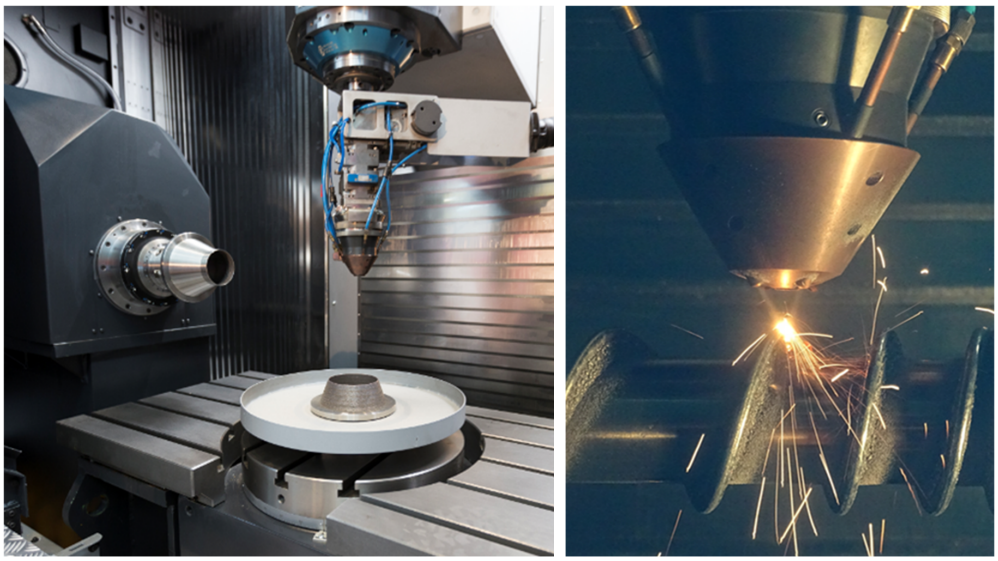

(**a**) (b)

Figure 11. (**a**) IBARMIA ZVH45/1600 Add + Process hybrid machine; (**b**) four-stream discrete coaxial nozzle.

2.2.2. Strategy Development and Experimental Validation

Optimum working conditions (P, v, $\dot{m}_p$), which were obtained from previous works [25], were selected for Alloy 718 deposition with a four-stream nozzle. All other processing variables were held constant during the experimentation, while considering previous experience. The optimum working distance and laser spot diameter were obtained in the same way as Tabernero et al. [31], as described by Artaza et al. [32]. Their methodology consisted of using containers with different internal diameters for trapping the powder from the powder stream and for measuring the amount of powder collected in each container at different distances from the nozzle [28]. The optimum distance (the distance that collected a higher amount of powder) obtained with that methodology was 14.5 mm for the discrete nozzle. Argon was employed as both a carrier and protective gas, at flow rates of 4.5 and 18 L·min^{-1}, respectively, while using a laser spot size of 2.6 mm. The rotation percentage of the powder feeder defines different powder mass flow rates, depending on the fluidity and the density of the powder material. The relation between the powder feeder rotating disk speed percentage and the powder mass flow rate was measured by weighing the powder that was collected within three minutes.

The trajectory to obtain the geometry depicted in Figure 10a was programmed employing Spyder software, while using a constant vertical (ΔZ) and horizontal (ΔX) displacement. The number of clads per layer excluding the extra clads (N_c) were selected by adjusting the overlapped ratio between 40 and 60%, for its adaptation to the shape of the wall. The results of the coating model at the parameters that were used in this validation showed that the waviness of the coating was considered to be excessive

at d_o less than 40%, and that the dilution depth was excessively low at higher value of 60%, with a risk of low substrate fusion. The trajectory program added one clad to the coating when the overlap percentage was lower than 40%. The average value of the growth per layer (ΔZ) was employed for the trajectory (Table 2).

Table 2. Parameters of each layer and average value. Overlap percentage (d_o), number of clads per layer (N_c) and layer height predicted by the model (H_L).

Layer	d_o (%)	N_c	H_L
1	50	3	1.3
2	42.2	3	1.1
3	56.3	4	1.5
4	51	4	1.3
5	59.4	5	1.6
6	55.5	5	1.4
7	51.6	5	1.3
8	47.7	5	1.2
9	55	6	1.4
10	51.9	6	1.3
11	48.8	6	1.3
12	45.7	6	1.1
Average	51.4	4.8	1.3

The process parameters to add the extra clads on the edges must be calculated as a function of the area that is needed for straight growth that varies with the overlap percentage, as previously shown in Figure 7. The simplest way to obtain them is to adapt the feed rate, maintaining the same laser power and powder mass flow rate. This occurs because the area of the single clad presents a linear trend with the inverse of the feed rate [13,27]. In this case, the trend of the single clad area, at the selected process parameters, with regard to controlled overlap percentage, can be considered to be linear in the range of 40 to 60% (Figure 12), simplifying the calculation of the extra clad area to a mean value (Table 2) that was used for calculating the extra clad feed rate. Thus, an extra clad was deposited every two layers with twice the area per layer, in order to obtain an extra clad with a feed rate as similar as possible to the coated clads (thus, similar efficiency). The strategy of deposition was a zig-zag strategy, which was based on the cladding path R2 of Kono et al. [23] (Figure 13) and the feed rate of the extra clad differed on each on the side of the wall. The extra clad area in the first clad side was 440 mm·min^{-1} (straight part) and the other edge feed rate was 500 mm·min^{-1}. Table 3 summarizes the main parameters.

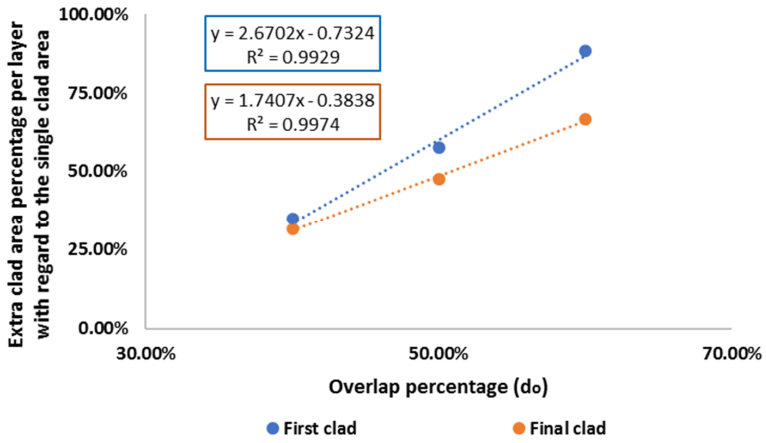

Figure 12. Representation of the extra clad area needed to compensate the lack of material on the edges of the layer as a function of the overlap percentage. Linear trend of the extra clad area in the range of a 40% to 60% overlap with the parameters from Table 3.

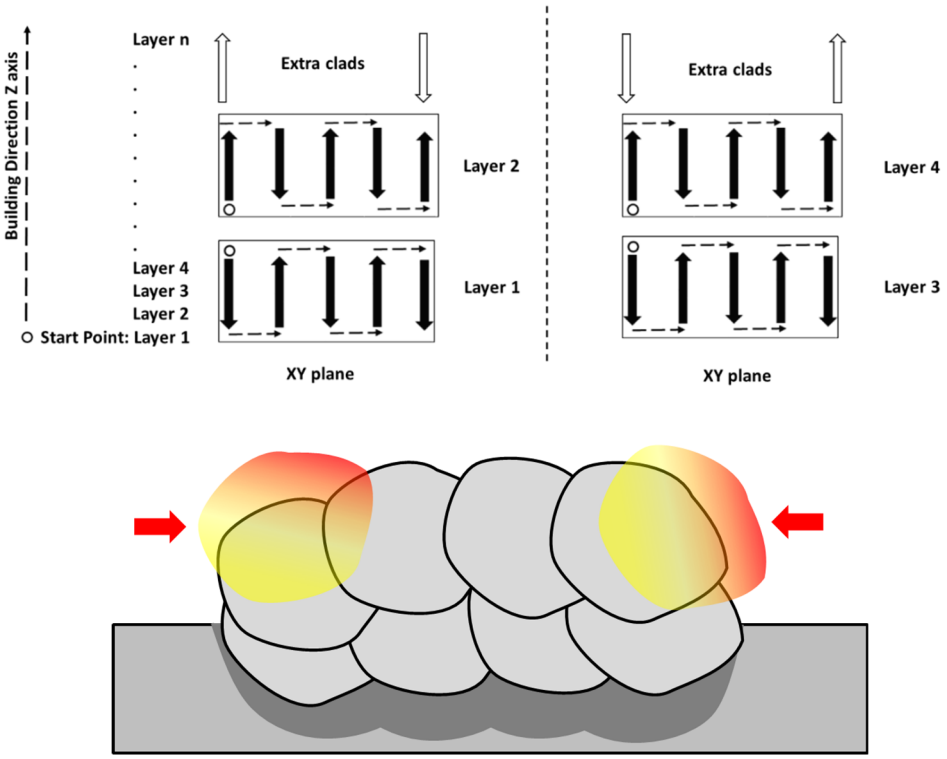

Figure 13. Scheme of the extra clad deposition strategy validation during the manufacturing of a wall.

Table 3. Validation strategy of Alloy 718 variable thickness walls. Main deposition parameters.

P (W)	v (mm·min^{-1})	$\dot{m}_p$ (g·min^{-1})	d_o (%)	ΔZ (mm)	ΔX (mm)	θ (°)	η_p (%)
2500	500	18	40–60	1.3	0.58	66	60

3. Results and Discussion

The wall deposited with variable overlapping and extra clad strategy presented the predicted geometric shape with low distortions at the edge and a total wall height that was close to expected with low variability. The cross section was measured employing Clemex Captiva® image analyzer software (Clemex, Longueuil, QC, Canada). The analyzed cross section presented waviness and differences with the theoretical dimensions (Figure 14), but the variable overlap percentage was sufficient for fixing the deposited material at the expected geometry and the extra clad strategy provided stable growth.

The sloped side presented maximum dimensional deviations on the horizontal axis, in relation with the target geometry of 0.51 mm and −0.48 mm, on a line where the negative value represents a lack of material. The straight side presented maximum deviations on the horizontal axis regarding the target geometry of 0.67 mm and −0.16 mm. The maximum and minimum height on the vertical axis generated maximum deviations in relation with the target value of 1.14 mm and −0.79 mm. The results mean a maximum deviation of 7.3% and −5% from the target height. Regarding the deposited area, 6.95% of its total area was deposited outside the theorical geometry: 2.44% of the area on the straight side of the wall, 0.73% on the inclined side of the wall, and 3.78% within the zone of excess height. Despite the observed deviations, the deposited area can be considered to be very similar to the target area, so it can be concluded that the efficiency of the single clad remained constant when manufacturing both coatings and multilayer structures.

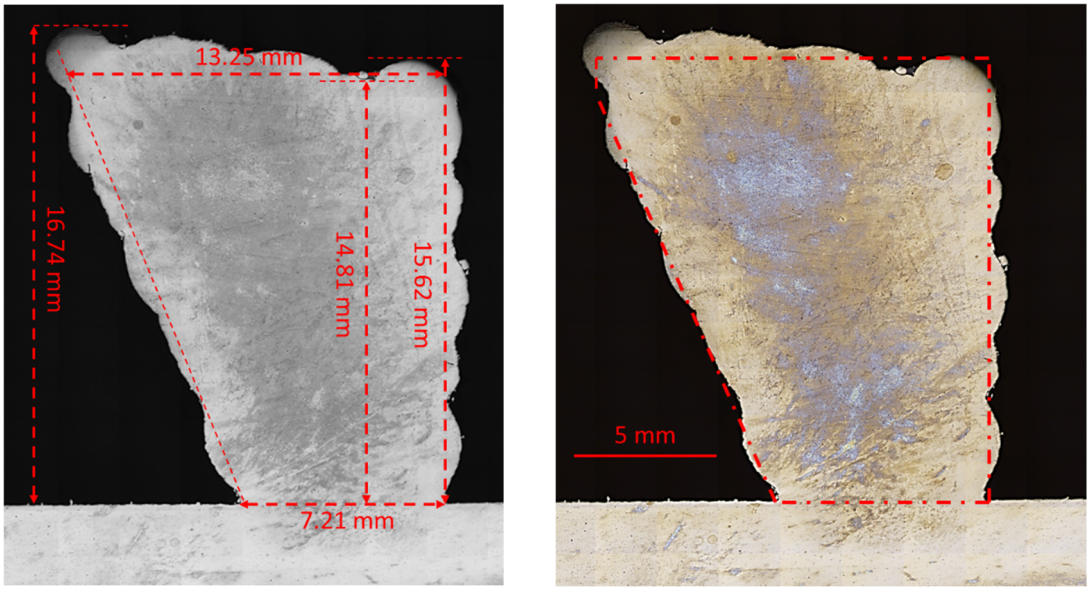

(**a**) (**b**)

Figure 14. Cross section: (**a**) dimensions; (**b**) compared with the Computer Aided Design (CAD).

The results also suggest that it would be necessary to fabricate the geometry by DED with an extra thickness on the horizontal axis with at least the value of the dimensional differences related to the lack of material and with a higher extra height of at least 5% in order to obtain the target geometry after machining. The maximum dimensional differences that were related to an excess of material were then considered as the starting point for subsequent machining process. Thus, a considerable variation in cutting force in relation to the material removal rate might be expected during the first machining pass, due to the waviness of the wall, as Ostra et al. observed [33]. There is the possibility of obtaining different parameters in order to improve the geometry (e.g. lower height per layer or lower laser power in an attempt to reduce waviness), but, depending on the process parameters, the efficiency and productivity of the DED could decrease. Thus, any savings in the machining process need to be carefully balanced with the efficiency and the productivity losses within the DED process.

Although the strategy was validated and it was possible to obtain acceptable accuracy in the deposited geometry employing the information of the geometrical model and reducing the quantity of experimental runs, the waviness that was observed in the structure and the differences obtained for its height, highlighted the need for in-process controls, in order to improve the geometry. In this sense, there are already commercially available in-process controls for minimizing the variability of the powder fed DED process, such as those that were developed in the frame of the largest EU Research and Innovation program Horizon 2020. These controls are focused on controlling the melt pool size through laser power control or layer height based on the regulation of the feed rate. The first control corrects instabilities that are related with an excess of heat input and the latter corrects instabilities related with the amount of material deposited per layer. Thus, the selection of one type or a mix of both controls depends on both the application and the power supply. Some examples are the CLAMIR system for DED and cladding process control (New Infrared Technologies, Madrid, Spain) and the height control that was developed by Siemens employing a Precitec sensor (Siemens, Munich, Germany) [34,35].

To complete the study, a cross section of the wall (Figure 15a) was cut, ground, polished, and etched with an oxidic acid solution, in order to analyze both its structure and its defects. The structure presented no cracks and only a few isolated pores with diameters under 25 µm were found in the cross section under analysis (Figure 15b). The need for HIP treatment would depend on the porosity percentage specifications, depending on the application requirements, as in the work of Zhong et al. [36].

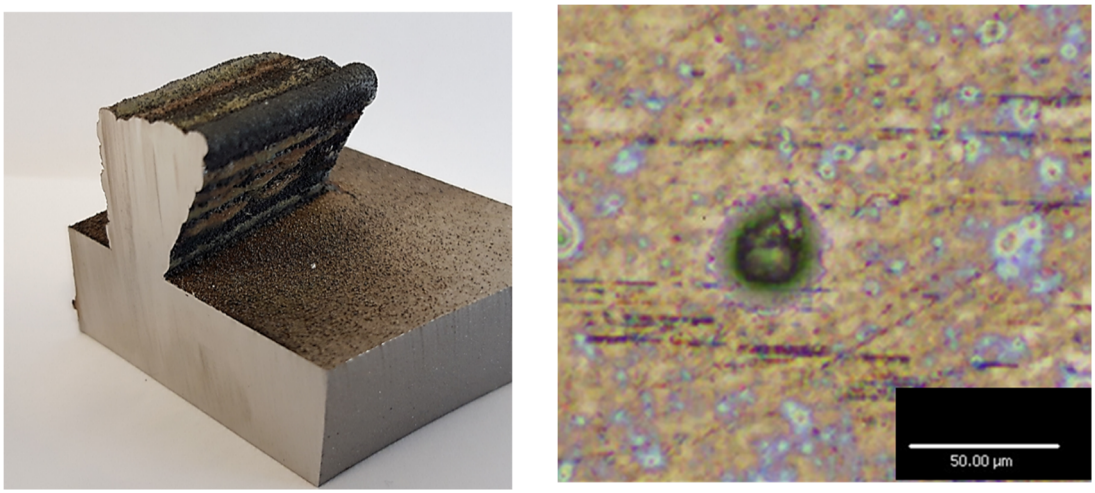

(**a**) (**b**)

Figure 15. Results: (**a**) variable thickness wall cut in different cross sections for analyzing the structure and the geometrical dimensions; (**b**) pore of less than 25 µm.

The wall presented long columnar grains, as in the work of Ostra et al. [33], so mechanical property anisotropy may be expected, unfavorable residual stresses, a sharp reduction of the elongation, and higher hardness in comparison with the same forged and sol-annealed material. This structure could increase the wear resistance in coating applications, although it reduces the fatigue lifetime, due to premature crack initiation, as commented on by Lewandowski et al. [37]. Thus, a subsequent heat treatment process might be necessary, as in the work of Zhang et al. [38], in order to improve the material properties, transform the columnar grains into equiaxed grains, and eliminate material anisotropy by homogenization before aging treatments and subsequent machining.

4. Conclusions

The main conclusions of this study can be summarized, as follows:

- The proposed model and deposition strategy for multilayered walls of variable thickness deposited on horizontal substrate by using only the single clad characteristics as inputs, the overlap percentage and the tilting angle have been validated.
- In the proposed strategy, a different feed rate is needed for the extra clad, depending on the edge where it is deposited. Changing the overlap percentage per layer in the selected range adapted the deposited material to the geometry.
- Although the strategy was correct and it was possible to obtain acceptable accuracy in the deposited geometry, the waviness that was observed in the structure and the different heights that were obtained highlighted the need for an in-process control.

It is clear that a geometrical model cannot replace the numerical model of the heat transfer and fluid flow in the DED process, but it could facilitate the work of the control system and rapidly establish an expected geometry and the best deposition strategy. It can be also helpful for designers to understand and select the parameters, depending on the dimensional requirements of the coating, such as effective thickness, dilution, and layer height, and to select the subsequent machining strategy that is based on the predicted geometry of the model. Thus, both finite elements based numerical models and geometrical models can be considered to be complementary.

In future works, the models developed here could be applied in Computer-Aided Manufacturing software, in order to calculate the DED process toolpath, the Computer Assisted Design expected from the DED process, and the subsequent machining toolpath.

Author Contributions: Conceptualization, P.R., M.O. and A.A.; methodology, P.R., A.A. and A.L.; software, P.R.; validation, P.R. and M.O.; formal analysis, P.R.; investigation, P.R.; resources, A.A. and A.L.; data curation, P.R.; writing—original draft preparation, P.R.; writing—review and editing, P.R., M.O. and A.A.; visualization, P.R.; supervision, A.A. and A.L.; project administration, A.A. and A.L.; funding acquisition, A.A. All authors have read and agreed to the published version of the manuscript.

Funding: This research was funded by the European Commission through the project "PARADDISE: a Productive, Affordable and Reliable solution for large scale manufacturing of metallic components by combining laser-based Additive and Subtractive processes with high Efficiency" (Grant Agreement 723440), an initiative of the Public-Private Partnership "Photonics and Factories of the Future". This research was also funded by European Institute of Innovation & Technology (EIT) through the project "DEDALUS: Directed Energy Deposition machines with integrated process ALgorithms Under dedicated monitoring and control System" (ID 20094) and by the vice-counseling of technology, innovation and competitiveness of the Basque Government (Eusko Jaurlaritza) under the ELKARTEK Program, PROCODA and QUALYFAM projects, grant number KK-2019/00004 and KK-2020/00042, respectively.

Conflicts of Interest: The authors declare no conflict of interest. The funders had no role in the design of the study; in the collection, analyses, or interpretation of data; in the writing of the manuscript, or in the decision to publish the results.

Nomenclature

Symbol	Description	Unit
a	Coefficient of the equation of the second-degree parabola	-
A	Area	mm^2
A_o	Overlapped area of clad i	mm^2
A_T	Layer area	mm^2
A'	Area of clad $i + 1$	mm^2
b	Coefficient of the equation of the second-degree parabola	-
DED	Directed Energy Deposition	-
d_o	Overlap percentage between adjacent clads	%
D_o	Distance between center lines of adjacent clads	mm
h	Height	mm
H_L	Layer height	mm
i	Number of the clad in the coating	-
L_c	Length of the coating	mm
MDR	Mass Deposition Rate	$Kg{\cdot}h^{-1}$
$\dot{m}_p$	Powder mass flow rate	$g{\cdot}min^{-1}$
N_C	Number of clads per layer	-
N_L	Number of layers of the wall	-
O	Origin	-
p	Dilution depth	mm
P	Laser power	W
v	Feed rate	$mm{\cdot}min^{-1}$
w	Width	mm
x	X axis	-
y	Y axis	-
Y_i	Overlap point height	mm
ΔX	Horizontal displacement	mm
ΔZ	Vertical displacement	mm
η_p	Efficiency of the injected powder	%
θ	Wall angle	°

References

1. Mehrpouya, M.; Dehghanghadikolaei, A.; Fotovvati, B.; Vosooghnia, A.; Emamian, S.S.; Gisario, A. The Potential of Additive Manufacturing in the Smart Factory Industrial 4.0: A Review. *Appl. Sci.* **2019**, *9*, 3865. [CrossRef]
2. Szymczyk-Ziółkowska, P.; Łabowska, M.B.; Detyna, J.; Michalak, I.; Gruber, P. A review of fabrication polymer scaffolds for biomedical applications using additive manufacturing techniques. *Biocybern. Biomed. Eng.* **2020**, *40*, 624–638. [CrossRef]
3. Ning, J.; Sievers, D.E.; Garmestani, H.; Liang, S.Y. Analytical modeling of in-situ deformation of part and substrate in laser cladding additive manufacturing of Inconel 625. *J. Manuf. Process.* **2020**, *49*, 135–140. [CrossRef]
4. Cortina, M.; Arrizubieta, J.I.; Ruiz, J.E.; Ukar, E.; Lamikiz, A. Latest Developments in Industrial Hybrid Machine Tools that Combine Additive and Subtractive Operations. *Materials* **2018**, *11*, 2583. [CrossRef]
5. Tamanna, N.; Crouch, R.; Naher, S. Progress in numerical simulation of the laser cladding process. *Opt. Lasers Eng.* **2019**, *122*, 151–163. [CrossRef]
6. Salonitis, K.; D'Alvise, L.; Schoinochoritis, B.; Chantzis, D. Additive manufacturing and post-processing simulation: Laser cladding followed by high speed machining. *Int. J. Adv. Manuf. Technol.* **2016**, *85*, 2401. [CrossRef]
7. Arrizubieta, J.I.; Lamikiz, A.; Cortina, M.; Ukar, E.; Alberdi, A. Hardness, grainsize and porosity formation prediction on the Laser Metal Deposition of AISI 304 stainless steel. *Int. J. Mach. Tools Manuf.* **2018**, *135*, 53–64. [CrossRef]
8. Wei, H.; Knapp, G.; Mukherjee, T.; Debroy, T. Three-dimensional grain growth during multi-layer printing of a nickel-based alloy Inconel 718. *Addit. Manuf.* **2019**, *25*, 448–459. [CrossRef]
9. Lu, X.; Lin, X.; Chiumenti, M.; Cervera, M.; Hu, Y.; Ji, X.; Ma, L.; Yang, H.; Huang, W. Residual stress and distortion of rectangular and S-shaped Ti-6Al-4V parts by Directed Energy Deposition: Modelling and experimental calibration. *Addit. Manuf.* **2019**, *26*, 166–179. [CrossRef]
10. Dass, A.; Moridi, A. State of the Art in Directed Energy Deposition: From Additive Manufacturing to Materials Design. *Coatings* **2019**, *9*, 418. [CrossRef]
11. Azarniya, A.; Garmendia, X.; Mirzaali, M.J.; Sovizi, S.; Bartolomeu, F.; Mare, K.S.W.; Wits, W.W.; Yap, C.Y.; Ahn, J.; Miranda, G.; et al. Additive manufacturing of Ti–6Al–4V parts through laser metal deposition (LMD): Process, microstructure, and mechanical properties. *J. Alloy. Compd.* **2019**, *804*, 163–191. [CrossRef]
12. De Oliveira, U.; Ocelík, V.; De Hosson, J.T.M. Analysis of coaxial laser cladding processing conditions. *Surf. Coat. Technol.* **2005**, *197*, 127–136. [CrossRef]
13. Ramiro, P.; Alberdi, A.; Ortiz, M.; Lamikiz, A.; Ukar, E. Characteristics of Fe-, Ni- and Co-based powder coatings fabricated by laser metal deposition without preheating the base material. *Procedia CIRP* **2018**, *68*, 381–386. [CrossRef]
14. El Cheikh, H.; Courant, B.; Branchu, S.; Huang, X.; Hascoët, J.Y.; Guillén, R. Direct Laser Fabrication process with coaxial powder projection of 316L steel. Geometrical characteristics and microstructure characterization of wall structures. *Opt. Laser Eng.* **2012**, *50*, 1779–1784. [CrossRef]
15. Arregui, L.; Garmendia, I.; Pujana, J.; Soriano, C. Study of the Geometrical Limitations Associated to the Metallic Part Manufacturing by the LMD Process. *Procedia CIRP* **2018**, *68*, 363–368. [CrossRef]
16. Möller, M.; Baramsky, N.; Ewald, A.; Emmelmann, C.; Schlattmann, J. Evolutionary-based Design and Control of Geometry Aims for AMD-manufacturing of Ti-6Al-4V Parts. *Phys. Procedia* **2016**, *83*, 733–742. [CrossRef]
17. Hao, J.; Meng, Q.; Li, C.; Li, Z.; Wu, D. Effects of tilt angle between laser nozzle and substrate on bead morphology in multi-axis laser cladding. *J. Manuf. Process.* **2019**, *43*, 311–322. [CrossRef]
18. Bax, B.; Rajput, R.; Kellet, R.; Reisacher, M. Systematic evaluation of process parameter maps for laser cladding and directed energy deposition. *Addit. Manuf.* **2018**, *21*, 487–494. [CrossRef]
19. El Cheikh, H.; Courant, B.; Branchu, S.; Hascoët, J.Y.; Guillén, R. Analysis and prediction of single laser tracks geometrical characteristics in coaxial laser cladding process. *Opt. Lasers Eng.* **2012**, *50*, 413–422. [CrossRef]
20. Chen, T.; Wu, W.; Li, W.; Liu, D. Laser cladding of nanoparticle TiC ceramic powder: Effects of process parameters on the quality characteristics of the coatings and its prediction model. *Opt. Laser Technol.* **2019**, *116*, 345–355. [CrossRef]

21. Zhang, K.; Wang, S.; Liu, W.; Shang, X. Characterization of stainless steel parts by Laser Metal Deposition Shaping. *Mater. Design* **2014**, *55*, 104–119. [CrossRef]
22. Garmendia, I.; Leunda, J.; Pujana, J.; Lamikiz, A. In-process height control during laser metal deposition based on structured light 3D scanning. *Procedia CIRP* **2018**, *68*, 375–380. [CrossRef]
23. Kono, D.; Maruhashi, A.; Yamaji, I.; Oda, Y.; Mori, M. Effects of cladding path on workpiece geometry and impact toughness in Directed Energy Deposition of 316L stainless steel. *CIRP Ann.* **2018**, *67*, 233–236. [CrossRef]
24. Ramiro, P.; Ortiz, M.; Alberdi, A.; Lamikiz, A. Geometrical Model and Strategy in Single and Multilayer Structures Deposited by Powder-Fed Directed Energy Deposition. *Procedia CIRP* **2020**, *94*, 352–356. [CrossRef]
25. Ramiro-Castro, P.; Ortiz, M.; Alberdi, A.; Lamikiz, A. Effects of Gravity and Non-Perpendicularity during Powder-Fed Directed Energy Deposition of Ni-Based Alloy 718 through Two Types of Coaxial Nozzle. *Metals* **2020**, *10*, 560. [CrossRef]
26. Ocelík, V.; Nenadl, O.; Palavra, A.; De Hosson, J.T.M. On the geometry of coating layers formed by overlap. *Surf. Coat. Technol.* **2014**, *242*, 54–61. [CrossRef]
27. Ramiro, P.; Ortiz, M.; Alberdi, A.; Lamikiz, A. Characteristics of Fe-based powder coatings fabricated by laser metal deposition with annular and four stream nozzles. *Procedia CIRP* **2018**, *74*, 201–205. [CrossRef]
28. Ramiro, P.; Ortiz, M.; Alberdi, A.; Lamikiz, A. Optimization of the efficiency of the laser metal deposition process applied to high hardness coatings by the analysis of different types of coaxial nozzles. *DYNA* **2018**, *93*, 613–619. [CrossRef]
29. Chakraborty, S.S.; Dutta, S. Estimation of dilution in laser cladding based on energy balance approach using regression analysis. *Sādhanā* **2019**, *44*, 150. [CrossRef]
30. Nenadl, O.; Kuipers, W.; Koelewijn, N.; Ocelík, V.; De Hosson, J.T.M. A versatile model for the prediction of complex geometry in 3D direct laser deposition. *Surf. Coatings Technol.* **2016**, *307*, 292–300. [CrossRef]
31. Tabernero, I.; Lamikiz, A.; Ukar, E.; López de Lacalle, L.N.; Angulo, C.; Urbikain, G. Numerical simulation and experimental validation of powder flux distribution in coaxial laser cladding. *J. Mater. Process. Technol.* **2010**, *210*, 2125–2134. [CrossRef]
32. Artaza, T.; Ramiro, P.; Ortiz, M.; Alberdi, A.; Lamikiz, A. Effects of the Nozzle Tip Clogging and the Scanning Direction on the Deposition Process During Laser Metal Deposition of Alloy 718 Using a Four-Stream Discrete Nozzle. *Procedia Manuf.* **2019**, *41*, 264–271. [CrossRef]
33. Ostra, T.; Alonso, U.; Veiga, F.; Ortiz, M.; Ramiro, P.; Alberdi, A. Analysis of the Machining Process of Inconel 718 Parts Manufactured by Laser Metal Deposition. *Materials* **2019**, *12*, 2159. [CrossRef] [PubMed]
34. 3D printing media network. Available online: https://www.3dprintingmedia.network/clamir-process-control-system-nit-powers-lmd-3d-printing/ (accessed on 1 May 2020).
35. New Siemens. Available online: https://new.siemens.com/global/en/company/stories/research-technologies/additivemanufacturing/additive-manufacturing-laser-metal-deposition.html (accessed on 1 May 2020).
36. Zhong, C.; Gasser, A.; Kittel, J.; Wissenbach, K.; Poprawe, R. Improvement of material performance of Inconel 718 formed by high deposition-rate laser metal deposition. *Mater. Design* **2016**, *98*, 128–134. [CrossRef]
37. Lewandowski, J.J.; Seifi, M. Metal additive manufacturing: A review of mechanical properties. *Annu. Rev. Mater. Res.* **2016**, *46*, 151–186. [CrossRef]
38. Zhang, Y.; Yang, L.; Chen, T.; Zhang, W.; Huang, X.; Dai, J. Investigation on the optimized heat treatment procedure for laser fabricated IN718 alloy. *Opt. Laser Technol.* **2017**, *97*, 172–179. [CrossRef]